Biochimica et Biophysica Acta 1817 (2012) 526–536

Contents lists available at SciVerse ScienceDirect

Biochimica et Biophysica Acta

journal homepage: www.elsevier.com/locate/bbabio

Review

Proton-pumping mechanism of cytochrome *c* oxidase: A kinetic master-equation approach ☆

Young C. Kim [a,*], Gerhard Hummer [b,**]

[a] Center for Computational Materials Science, Naval Research Laboratory, Washington, DC, 20375, USA
[b] Laboratory of Chemical Physics, National Institute of Diabetes and Digestive and Kidney Diseases, National Institutes of Health, Bethesda, MD 20892-0520, USA

ARTICLE INFO

Article history:
Received 18 May 2011
Received in revised form 31 August 2011
Accepted 6 September 2011
Available online 16 September 2011

Keywords:
Proton pumping
Cytochrome *c* oxidase
Respiratory chain
Energy transduction
Molecular machine
Kinetic master equation

ABSTRACT

Cytochrome *c* oxidase is an efficient energy transducer that reduces oxygen to water and converts the released chemical energy into an electrochemical membrane potential. As a true proton pump, cytochrome *c* oxidase translocates protons across the membrane against this potential. Based on a wealth of experiments and calculations, an increasingly detailed picture of the reaction intermediates in the redox cycle has emerged. However, the fundamental mechanism of proton pumping coupled to redox chemistry remains largely unresolved. Here we examine and extend a kinetic master-equation approach to gain insight into redox-coupled proton pumping in cytochrome *c* oxidase. Basic principles of the cytochrome *c* oxidase proton pump emerge from an analysis of the simplest kinetic models that retain essential elements of the experimentally determined structure, energetics, and kinetics, and that satisfy fundamental physical principles. The master-equation models allow us to address the question of how pumping can be achieved in a system in which all reaction steps are reversible. Whereas proton pumping does not require the direct modulation of microscopic reaction barriers, such kinetic gating greatly increases the pumping efficiency. Further efficiency gains can be achieved by partially decoupling the proton uptake pathway from the active-site region. Such a mechanism is consistent with the proposed Glu valve, in which the side chain of a key glutamic acid shuttles between the D channel and the active-site region. We also show that the models predict only small proton leaks even in the absence of turnover. The design principles identified here for cytochrome *c* oxidase provide a blueprint for novel biology-inspired fuel cells, and the master-equation formulation should prove useful also for other molecular machines. This article is part of a Special Issue entitled: Respiratory Oxidases.

Published by Elsevier B.V.

1. Introduction

Cytochrome *c* oxidase (CcO) is the terminal enzyme in the respiratory electron transport chain of mitochondria (or bacteria) located in the inner mitochondrial (or bacterial) membrane. It catalyzes the reduction of oxygen to water to generate the electrochemical proton gradient across the membrane that powers the production of ATP. The enzyme takes up four electrons from the positively charged P side (outside) of the membrane and four protons from the negatively charged N side (inside) for the reduction of dioxygen to two water molecules [1–10],

$$4e^-_{out} + 8H^+_{in} + O_2 \rightarrow 2H_2O + 4H^+_{out}. \quad (1)$$

Coupled to this oxygen reduction reaction, four additional protons are translocated from the N side to the P side across the membrane against an opposing membrane potential, doubling the total amount of charge separated by the enzyme. Since the discovery of this remarkable and then unexpected CcO proton pumping activity [1], extensive studies using a wide variety of biophysical and biochemical techniques in combination with site-directed mutagenesis and X-ray crystallography as well as theory and computation have greatly advanced our understanding of the function of CcO [4,6,9–27]. However, key aspects of the fundamental mechanisms underlying the redox-coupled proton pumping remain unclear.

Charge separation across the membrane is achieved in CcO by two separate processes. First, the reduction of oxygen to water by electrons and protons taken up from opposite sides of the membrane leads to the net translocation of one electrical charge across the membrane per electron consumed, in accordance with the celebrated Lundegårdh–Mitchell redox loop model [28]. Second, an additional proton is translocated vectorially across the membrane for each electron consumed, resulting in a net transport of two electrical charges per electron. This redox-coupled proton pumping has been a central issue in bioenergetics, and many models have been proposed to explain its mechanism [4,6,11,15–18,21–24,29]. Although these models were constructed to reflect the intermediate states of redox chemistry

☆ This article is part of a Special Issue entitled: Respiratory Oxidases.

* Corresponding author.
** Corresponding author. Tel.: +1 301 402 6290; fax: +1 301 496 0825.
E-mail addresses: youngchan.kim@nrl.navy.mil (Y.C. Kim), gerhard.hummer@nih.gov (G. Hummer).

0005-2728/$ – see front matter. Published by Elsevier B.V.
doi:10.1016/j.bbabio.2011.09.004

occurring inside CcO as well as some key reaction steps, they by and large fail to address the following fundamental question: How is the energy released from the redox chemistry of oxygen utilized to translocate protons unidirectionally, in particular, in the presence of possible proton leakage driven by the opposing membrane potential?

Answers to this central question require a basic understanding of molecular machines that operate in a microscopic environment where thermal motion is non-negligible. Although the Laws of Thermodynamics, including the Second Law of Thermodynamics, were formulated originally for macroscopic systems where fluctuations of thermodynamic variables can be ignored, they do apply to microscopic molecular machines, such as CcO or motor proteins. Taking these principles into account is relevant also for the development of biology-inspired nanoscale molecular machines [30–33] that retain one of the most remarkable aspects of biomolecular machines, their high efficiency of operation in environments subject to thermal noise. To address these challenges, physics-based stochastic and network models have been proposed to describe biological molecular machines including motor proteins and biochemical reactions [34–40]. Such approaches are relevant also in bioenergetics, not least for the development of a more detailed understanding of the proton pumping activity of CcO.

Here we summarize and extend recent studies of redox-coupled proton pumping in CcO that employ stochastic kinetic models [41–43]. The models were constructed at the molecular level in accordance with basic physical principles and the overall architecture of CcO, with observed equilibria and rates for intermediate reaction steps, and with measured proton and electron affinities. A detailed analysis of the resulting kinetic models highlights the basic requirements for redox-driven proton pumping, and sheds light onto the molecular mechanism of the CcO proton pump. Kinetic gating emerges as an essential requirement for efficient pumping, which can be realized by proton delivery mechanisms that exploit a water-gate [21] and a Glu valve [44]. We conclude with a brief discussion of future directions and implications on other molecular machines.

2. Molecular machines and Maxwell's demon

Biological molecular machines are efficient energy transducers that convert electrical, chemical or light energy to other types of energy [45–47]. For example, motor proteins, such as myosins, kinesins and dyneins, utilize chemical energy released by ATP hydrolysis to perform mechanical work including muscle contraction, cargo transport and bacterial motion [48–50]. Ion channels, although not active energy transducers such as motor proteins, dissipate electrochemical potential gradients by passive translocation of charge across the membrane [51,52]. As part of the respiratory chain, ATP-synthase is a rotary motor that converts the proton gradient across the membrane generated by CcO and other respiratory protein complexes into chemical energy via ATP synthesis [53]. Despite the significant influence of thermal fluctuations at the microscopic level, many molecular machines exhibit remarkably high efficiency in energy transduction. This bodes well for various future applications in nanotechnology and medicine [31]. However, fundamental principles governing these remarkable machines are still under investigation.

The molecular machinery of life operates in conditions far from equilibrium. Whereas temperature can be thought of as spatially invariant at the cellular level, strong nonequilibrium conditions exist for the concentrations of ions and molecules. This nonequilibrium is reflected in the electrochemical potentials and concentration gradients across the membranes used by cells to compartmentalize space. In the development of thermodynamic descriptions of such systems, a central question is how the concentration nonequilibrium and the membrane potential can be established and maintained. This problem is akin to that raised by Maxwell's demon, which, in its original formulation, spontaneously creates a temperature-difference by sorting fast molecules from slow ones passing a microscopic door between two containers of gas. In an organism, the constant supply of foodstuff and the removal of the metabolic products drive the cellular machines toward steady state. To treat such an open system, we employ the tools of stochastic and network thermodynamics [34,36–40,54–56]. In this framework, a thermodynamically "uphill" reaction (here proton pumping) can be coupled to a "downhill" reaction (here oxygen reduction) that provides an overall driving force in conditions of controlled reactant concentrations.

3. Cytochrome *c* oxidase

CcO is responsible for reducing >90% of the oxygen taken up in aerobic life. For the reduction of dioxygen, CcO takes up four electrons from cytochrome *c* in the inter-membrane space of the mitochondria (or periplasmic side in bacteria), while four protons are taken up from the mitochondrial matrix (or the cytosol in bacteria). Fig. 1 presents the structure of the catalytic core consisting of subunits I–III from bovine CcO. The chemical reaction catalyzed by CcO results in a charge separation (one positive charge per electron consumed) across the membrane. In addition, four additional protons are transferred from the N side to the P side during the reaction, resulting in a total of two positive charges translocated across the membrane per electron consumed. The underlying chemical reaction is shown in Eq. (1). A wealth of details concerning CcO function has been revealed by biophysical and biochemical experiments. The redox chemistry of oxygen takes place in the binuclear center (BNC) located about one third from the P side of the membrane, which consists of heme a_3 and Cu_B (see Fig. 1). Four electrons are taken up from the cytochrome *c* at the P side via metal sites, Cu_A and heme *a*, and, in turn, are transferred to the BNC. Four protons for the chemical reaction are extracted from the N side of the membrane via two proton pathways, the D- and K-channels. The D-channel starts at a highly conserved residue, Asp 91 (bovine numbering; subunit I) near the N side, and continues to another highly conserved residue Glu 242 that donates

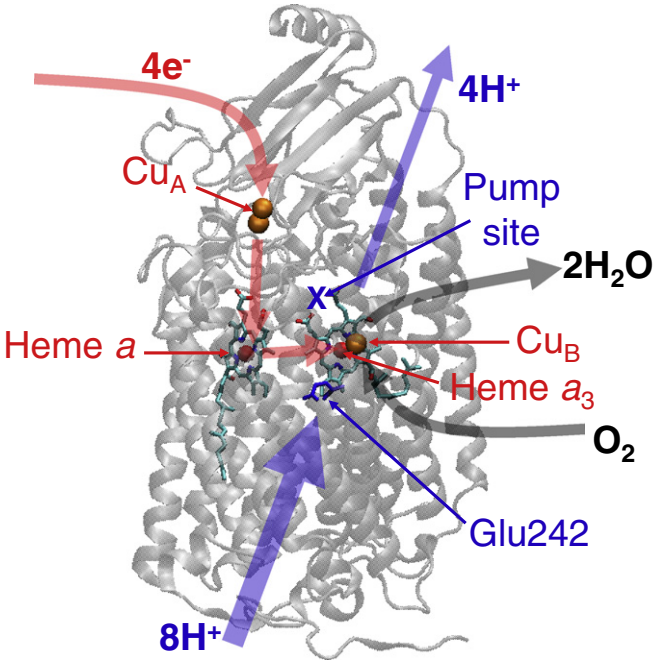

Fig. 1. Crystal structure [13] of the catalytic core formed by subunits I–III of the bovine cytochrome *c* oxidase. The redox centers (Cu_A, heme *a*, heme a_3, Cu_B) and proton sites (Glu 242 and unknown pump site) are shown explicitly. The electron and proton pathways are indicated by red and blue arrows, respectively. The gray arrows indicate the incoming dioxygen and the outgoing water released as a result of the redox chemistry occurring in the binuclear center (formed by heme a_3 and Cu_B).

protons to the BNC. The key residue in the K-channel is a highly conserved lysine (K319), which has been implicated in the delivery of the proton used in dioxygen bond-breaking [57,58]. It was suggested that two of the four "chemical" protons per O_2 consumed are delivered via the K-channel.

It is generally believed that all four "pump" protons are delivered via the D-channel, in which the pump protons are transferred from Glu 242 to a pump or "loading" site above the BNC. These protons are then delivered to the P side via a proton-exit channel. This results in a conundrum in which Glu 242 at the end of the D-channel should sort "pump" protons from "chemical" protons. At a first glance, this seems to suggest that CcO acts akin to Maxwell's demon in violation of the Second Law of Thermodynamics. Furthermore, the detailed balance condition imposes that there should be a proton leakage from the P side along the exit channel, which, in the presence of opposing membrane potential, will be intensified. Of course, the energy released from the reduction of oxygen powers the translocation of the protons. But a fundamental question is: How does scalar redox chemistry lead to vectorial transport of protons across the membrane without violating fundamental physical principles?

4. Kinetic models for redox-driven proton pumps

Master-equation approaches based on stochastic kinetics have gained popularity in recent years as descriptions of molecular machines, single-molecule enzyme kinetics, and other biochemical reactions [37,54–56,59]. In the following we review the design principles, construction and analysis of kinetic master-equation models specifically developed for redox-coupled proton pumps [41–43]. We then use these models to address some of the fundamental questions in relation to the proton pumping driven by redox chemistry. We also extend the models to examine detailed molecular mechanisms.

4.1. Construction of kinetic models

Fig. 2A presents a general N-site kinetic model of a redox-coupled proton pump with N_p proton and N_e electron sites ($N = N_p + N_e$). Each site can be occupied by only a single proton (blue circles) or electron (red squares), resulting in a total of 2^N microscopic states that are determined by the occupancy of the sites, $\mu = 1, 2, \ldots, N$. This binary state representation provides a more detailed description at the molecular level than the N "concentrations" one would have at the ensemble level. Two states i and j are kinetically connected (see arrows in Fig. 2A) if they are related through a single proton or electron transfer between sites, or between sites and the N (or P) side of the membrane. Note that Fig. 2A assumes a single proton channel connecting both sides of the membrane for demonstration purpose. However, multiple proton channels are observed in CcO, with its D and K channels, which can be incorporated into the model without difficulty. Also, multiple parallel proton or electron paths may be introduced between two sites within a channel. Detailed balance ensures that for a given forward reaction a backward reaction is allowed, as shown in Fig. 2A. To mimic the redox chemistry, we introduce special "active" sites for protons (M) and electrons (N), indicated in Fig. 2A in light colors. These sites participate in the "chemical reaction" in which a product is formed at a finite rate when the two sites are simultaneously occupied (see black arrows in Fig. 2A). Also the reverse chemical reaction is possible, as indicated in Fig. 2A (back arrow), with a rate determined by the redox equilibrium. Since the electron ends up reducing oxygen at the BNC in CcO, the last electron site N is always designated as the electron active site.

The kinetic scheme in Fig. 2A does not distinguish between the four reduction events in the dioxygen chemistry, Eq. (1). It assumes an infinite supply of electrons and protons, such that the overall concentrations of electrons and protons remain constant during the whole process. Also, it is assumed implicitly that the oxygen required for the redox chemistry is available instantly for chemical reaction. The product of the redox chemistry is constantly removed to avoid its build-up in the system, which would otherwise drive the reverse reaction and eventually result in equilibration. However, this assumption is not essential as long as the concentrations of reactants (protons, electrons, and oxygen) and product (water) are maintained at values far from equilibrium. This concentration nonequilibrium drives the open system into a steady state with nonzero electron and proton fluxes.

4.2. Rate coefficients and detailed balance

The rate coefficients between two kinetically connected states are constructed to satisfy detailed balance, except for the product formation reaction (black arrows in Fig. 2A). Specifically, let us consider two states i and j connected by a single proton or electron transfer between two sites or between a site and the N (or P) side of the membrane. Let k_{ji} (k_{ij}) be the transition rate coefficient from state i (j) to state j (i). Detailed balance then dictates that the ratio of forward

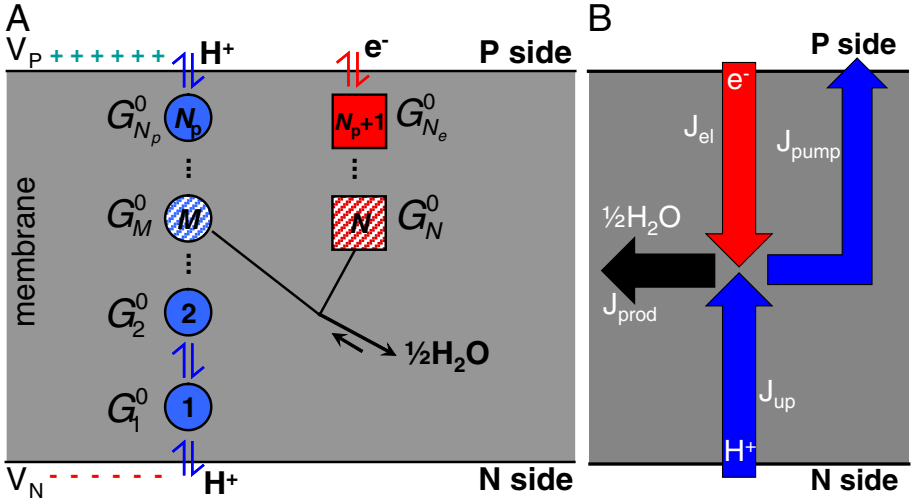

Fig. 2. (A) Schematic of an N-site kinetic model with N_p proton sites and N_e electron sites. Proton and electron sites are represented as blue circles and red squares, respectively, with corresponding intrinsic free energies. The light circle and square indicate active sites involved in product formation (black arrow). Vertical arrows indicate the allowed proton (blue) and electron (red) transfer reactions. (B) Flux diagram with net proton up-take flux, J_{up}, pump flux, J_{pump}, electron flux, J_{el}, and product flux, J_{prod}.
Adapted from Fig. 1 of Ref. [42].

and reverse rates is consistent with by the free energy difference between the two states, i.e.,

$$k_{ji}/k_{ij} = \exp\left[-\left(G_j - G_i\right)/k_B T\right], \tag{2}$$

where G_i is the free energy of state i, k_B is the Boltzmann constant, and T is the absolute temperature. Without loss of generality, the two rates can then be written as

$$k_{ji} = \kappa_{ij}\exp\left[-\alpha_{ij}\left(G_j - G_i\right)/k_B T\right], \tag{3}$$

$$k_{ij} = \kappa_{ij}\exp\left[+\left(1-\alpha_{ij}\right)\left(G_j - G_i\right)/k_B T\right], \tag{4}$$

where κ_{ij} is the intrinsic rate constant of the transition between states i and j in the absence of a thermodynamic driving force, i.e., $G_i = G_j$, while α_{ij} is a constant that distributes the contribution of the Boltzmann factor to forward and backward rates [54,56]. Note that the "load" distribution factor α_{ij} becomes relevant in the presence of external biases (here the membrane voltage), unless the symmetric matrix of prefactors $\kappa_{ij} = \kappa_{ji}$ is allowed to depend on the bias. Assuming linear free energy relations, the α_{ij} are related to the location of the respective transition state along the reaction path [55,56], as seen by rewriting Eqs. (3) and (4) in a more familiar Arrhenius form,

$$k_{ji} = \tau^{-1}\exp\left[-\left(G^*_{ij} - G_i\right)/k_B T\right], \tag{5}$$

$$k_{ij} = \tau^{-1}\exp\left[-\left(G^*_{ij} - G_j\right)/k_B T\right], \tag{6}$$

where G^*_{ij} is the free energy of the transition state between states i and j, and τ is a time constant. One can easily show that these two rate expressions are equivalent to

$$\kappa_{ij} = \tau^{-1}\exp\left[\left\{\alpha_{ij}G_j + \left(1-\alpha_{ij}\right)G_i - G^*_{ij}\right\}/k_B T\right]. \tag{7}$$

Note that in our previous studies of the kinetic models [41–43], α_{ij} was set equal to ½ independent of the states for simplicity even in the presence of a membrane potential. However, this constraint in general should be relaxed, or more generally κ_{ij} should be allowed to vary with voltage, despite the increase in the number of model parameters.

Product formation in the models (black arrows in Fig. 2A) is driven by a free energy gain of the redox chemistry corresponding to one quarter (~500 meV) of the energy released per electron consumed in dioxygen reduction. Thus, the forward product-formation rates contain an extra factor equal to $\exp(-\Delta G_p/k_B T)$ with $\Delta G_p = 500$ meV. This additional factor breaks the detailed balance between the forward/reverse product-formation rates, thus mimicking an open system in which the reactant and product concentrations are held constant. Ultimately, the broken detailed balance in the product formation step is responsible for generating a nonzero steady-state flux in the models.

The relative free energy G_i of state i is given by

$$G_i = \sum_{\mu=1}^{N} G^0_\mu x^{(i)}_\mu + \sum_{\mu=1}^{N-1}\sum_{\nu=\mu+1}^{N} \varepsilon_{\mu\nu} x^{(i)}_\mu x^{(i)}_\nu + \sum_{\mu=1}^{N} x^{(i)}_\mu q_\mu \frac{z_\mu V_m}{L} \tag{8}$$

where G^0_μ is the intrinsic relative free energy of site μ, and $\varepsilon_{\mu\nu}$ is the electrostatic coupling between two sites μ and ν determined by the effective Coulomb interactions of two charges in a planar low-dielectric membrane between two conducting media [60]. The occupancy variable $x^{(i)}_\mu$ is zero when site μ is empty in state i, and one when it is occupied. Here $V_m = V_P - V_N$ is the membrane potential, q_μ is the charge of site μ, z_μ is the distance from the N side of the membrane to site μ, and L is the membrane width taken to be 30 Å. Note, however, that care must be taken in assigning the voltage-dependent rate coefficients for proton and electron uptake, because of the broken symmetry of the two sides of the membrane in the presence of nonzero membrane voltage.

4.3. Master equation and pumping efficiency

The probability of state i, $P_i(t)$, as a function of time t satisfies the master equation

$$dP_i/dt = \sum_{j\neq i} k_{ij}P_j - \sum_{j\neq i} k_{ji}P_i, \tag{9}$$

where the first term on the right represents the incoming flux from all other states to state i, which is counterbalanced by the outgoing flux from state i to other states (second term). In the absence of the driving force ($\Delta G_p = 0$), the probabilities would approach equilibrium without any net flux, and satisfy the Boltzmann distribution, i.e., $P^{eq}_i/P^{eq}_j = \exp[-(G_i - G_j)/k_B T]$. For finite driving force ($\Delta G_p \neq 0$), the system approaches a steady state (i.e., $dP_i/dt = 0$) with steady-state probabilities, P^{ss}_i, obtained simply by solving the set of linear equations (9), with the left hand side set to zero. The net flux from state i to state j is then given by $J_{ij} = k_{ji}P^{ss}_i - k_{ij}P^{ss}_j$, which in turn results in an effective proton up-take flux, J_{up}, electron flux, J_{el}, pump flux, J_{pump}, and product flux, J_{prod}, as illustrated in Fig. 2B. The conservation of fluxes leads to $J_{el} = J_{up} = J_{pump} + J_{prod}$. We define the proton-pumping efficiency η as

$$\eta = \frac{J_{pump}}{J_{el}}, \tag{10}$$

which measures the average number of protons pumped per electron consumed. Note that the efficiency for separating charges across the membrane is then $1+\eta$. The pumping efficiency is related to the thermodynamic efficiency γ through

$$\gamma = (1+\eta)V_m/\Delta G_p, \tag{11}$$

which measures the efficiency of converting the chemical energy ΔG_p into electrical energy $(1+\eta)V_m$.

5. Principles of redox-driven proton pumping

Can kinetic models reveal general principles of proton pumping driven by the redox chemistry? Specifically, what are the basic requirements for a kinetic model that successfully pumps protons across the membrane? And under which conditions can a pump such as CcO operate efficiently in the presence of an opposing potential? To answer these questions, we explore the parameter space of the kinetic models in search of pumping solutions (with $\eta > 0$) by solving the master equation and optimizing the pumping efficiency. For a model with a given number of sites and rate coefficients k_{ij}, it is straightforward to find the steady-state solutions of Eq. (9). However, as the number of sites, N, increases, the total number of states as well as the number of parameters increases exponentially. In the most general case of a first-order kinetic system satisfying detailed balance, the number of free parameters is given by the sum of the states and the number of connections between them minus one. For the three-site model of pumping in Fig. 3A with eight states and $12+2=14$ connections, we thus end up with $8+14-1=21$ free parameters at any given voltage. For the five-site model of Fig. 3B, the number of free parameters is already >100. Thus for large N, it is difficult to explore the vast parameter space for pumping solutions and to analyze the solutions and extract any meaningful information from them. To understand basic principles of the redox-driven proton pumping, it is thus desirable to build models that are as simple as possible, but retain essential components of the redox-driven proton pump. On this premise, we have constructed the minimal model that is able to pump protons, and at the same time satisfies basic physical principles [41].

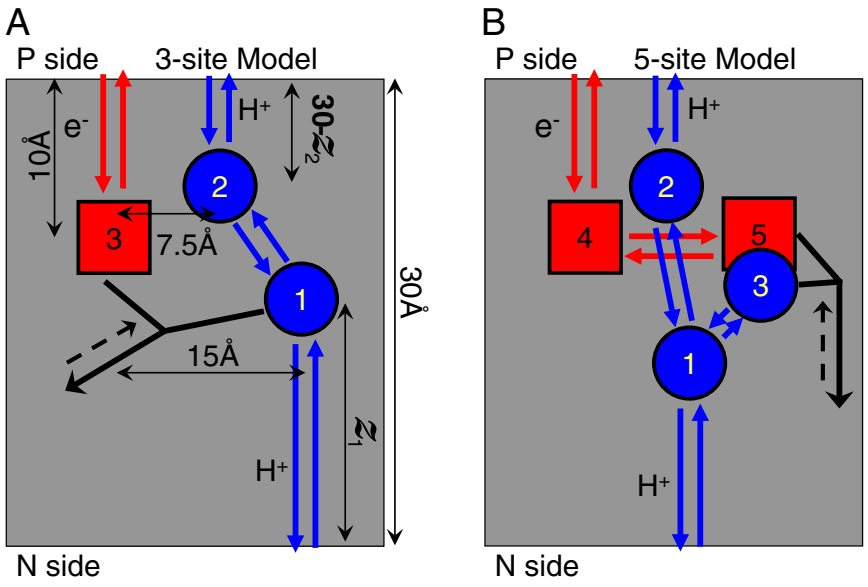

Fig. 3. Kinetic models of CcO. (A) Three-site model with two proton sites and one electron site and (B) five-site model with three proton sites and two electron sites. The arrows indicate the allowed transitions for protons (blue), electrons (red), and product formation (black).
Adapted from Fig. 1 of Ref. [42].

To achieve the proton-pumping function, the kinetic model requires a minimum of three sites: two proton sites and one electron site. It is straightforward to show that $N=2$ kinetic models (one for protons and the other for electrons) cannot pump protons across the membrane even in the absence of an opposing membrane voltage [41]. For $N=3$ models, two sites are necessary for protons in order to achieve pumping, which indicates that the complexity of proton pathways compared to electron pathways in CcO is critical for efficient proton pumping. In these models we had $M=1$, i.e., the N side is directly connected to the proton active site, which is separated by a "pump" (or proton loading) site 2 from the P side. Interestingly, when we reversed the order and placed the second proton site near the P side as the active site (i.e., $M=2$), we were not able to find any pumping solutions for a wide range of values in the parameter space. This result suggests that both the presence and the precise location of the pump site are essential for the efficiency of CcO. The pump site breaks the symmetry of the proton path, such that some of the protons taken up are pumped instead of consumed.

Electrostatic couplings between protons and electrons are key to proton pumping [17]. Indeed, at least for our $N=3$ models, it can be shown analytically, that electrostatic interactions between the sites are essential for proton pumping. Turning off the electrostatic interactions, either by introducing a high dielectric medium or by turning off the charges, eliminates the pumping ability. In addition, fine-tuning of the electrostatic interactions between various sites can greatly enhance the proton pumping efficiency as will be shown below. The importance of the electrostatic couplings in proton pumping can be understood by realizing that the electron taken up from the P side to the electron site is effectively modulating the energy landscape of a proton along the proton path connecting the N and P sides via electrostatic interactions. This tilting of the landscape is similar to the Brownian ratchet model proposed to describe the unidirectional motion of motor proteins via ATP hydrolysis, in which the chemical reaction that leads to the conformational change in the head domain alternates between two periodic free energy landscapes (with at least one being asymmetric) [38,39]. However, in our models of CcO, the "ratchet" controlling the landscape for proton transfer (pT) is itself a fluctuating part of the model.

The earlier study of the three-site models [41] showed that electrostatic couplings without any elaborate "gating" mechanism suffice to pump protons in the presence of opposing membrane voltage. More specifically, with $\alpha_{ij} = {}^1/_2$ and intrinsic rate coefficients κ_{ij} independent of microscopic states i and j, but dependent on the sites $\mu=1, 2, 3$ involved in the proton or electron transfer, release, or uptake reaction associated with the i–j transition, the restricted three-site models were able to pump protons *albeit* at a low efficiency ($\eta<0.2$) [41]. Also the models lost the pumping ability at membrane voltages >20 mV. In contrast, CcO can pump protons with efficiency close to 1 even at membrane voltages of ~200 mV. We showed that multiple redox sites present in CcO can improve the efficiency dramatically [41]. Furthermore, as we will show below, "kinetic gating" is essential to achieve high efficiency at larger membrane voltage within three-site models, which will provide insights into possible mechanisms of proton pumping by CcO.

6. Proton pumping mechanism of CcO

To understand the molecular mechanism of proton pumping by CcO, we aim to build a model that retains essential components of CcO and satisfies experimental data. In the following we examine kinetic models designed to mimic the architecture of CcO with thermodynamic constraints imposed to meet key experimental observations.

6.1. Building kinetic models for CcO

CcO contains a series of redox-active co-factors and conserved ionizable residues along the electron and proton transfer pathways that are crucial for its proton-pumping activity. Although it is, in principle, straightforward to include all these sites in building a kinetic model, the complexity of analyzing the solutions of the resulting master equation and the lack of data needed to determine unambiguous model parameters limit the possible gains in understanding of proton pumping mechanisms. Here we introduce two simple kinetic models for CcO that only retain the key redox and proton sites. The other sites are, in effect, integrated out and appear only implicitly in the form of effective rate coefficients. The simplest three-site model shown in Fig. 3A has a single electron site representing heme *a* and two proton sites corresponding to Glu 242 and a pump site. This model has been extensively investigated for its pumping mechanism. The less studied five-site model shown in Fig. 3B contains two electron sites (one for

heme *a* and the other for the BNC), and three proton sites (Glu 242, pump site and the BNC). This model, which resembles CcO more closely, however, has a total of $2^5 = 32$ states (compared to 8 states for the three-site model) and thus requires a large number of experimental data to determine its >100 transition rate coefficients. Even though it is straightforward to solve the master equation of the five-site model, lack of experimental data for the parameters thus makes it difficult to uncover the underlying mechanism of proton pumping. Therefore, in this review we will focus on the results obtained for the simplest three-site model. However, as we gather more information concerning the different reaction steps, as well as thermodynamic data, we believe that the more detailed five-site model will serve to better understand the mechanism of proton pumping by CcO.

6.2. Parameter values and experimental constraints

To make use of experimental data in the parameterization of the rate coefficients of our models, we first need to match individual reaction steps resolved experimentally to corresponding steps in the kinetic model, as illustrated in Fig. 4. We then employ a Monte Carlo (MC) search algorithm to identify regions of parameter space that result in acceptable values for the effective proton affinities, reaction rates, and equilibrium coefficients for intermediate reactions, as shown in Fig. 4A. For models that satisfy these experimental constraints, the MC search then aims to optimize the proton pumping efficiency. To prevent unrealistic values for the parameters and to cope with experimental observations, we imposed certain constraints on the parameters [42]. The intrinsic free energy, G^0_μ, of proton site μ is related to its intrinsic pK_a via

$$G^0_\mu = 2.3 k_B T \left(7 - pK^{int}_{a,\mu}\right), \tag{12}$$

while the midpoint potential of the electron site at the state i, ΔE^i_m, is given by

$$\Delta E^i_m = -25.6\left(G^0_3 + \sum_{\mu=1}^{2} x^{(i)}_\mu x^{(i)}_3 \varepsilon_{\mu 3}\right) \quad [\text{mV}]. \tag{13}$$

Based on experimental data of the apparent pK_a of Glu 242 [58,61,62], we restricted the pK_a of site 1 in the oxidized state to vary between 9 and 12, such that its intrinsic free energy is bounded by $-2.8 < G^0_1 < -6.9$ kcal/mol. The apparent pK_a of the pump site in the oxidized enzyme has been estimated to be 5.3 [9]. In our models, we limited the intrinsic free energy of site 2 to $1.4 < G^0_2 < 4.1$ kcal/mol, corresponding to pK_a values of the pump site between 4 and 6 in the oxidized state. Differences in the measured midpoint potentials of heme *a* (270 mV), Cu_A (250 mV), and cytochrome *c* (~270 mV) [9] were used only for model validation, not in model construction [42].

The electrostatic couplings, $\varepsilon_{\mu\nu}$, between the charge sites are determined by Coulomb interactions, $q_\mu q_\nu / D r_{\mu\nu}$, where D is the dielectric constant of the medium and $r_{\mu\nu}$ is the Euclidean distance between the sites μ and ν, augmented by the conducting boundary conditions on both ends of the membrane [60]. The geometry of the charge sites in the three-site model is presented in Fig. 3A, in which the electron site is fixed, while the two proton sites are allowed to move perpendicular to the membrane plane, with constraints that sites 1 and 2 remain below and above the electron site, respectively. The thermodynamic data indicate strong coupling between heme *a* and the pump site, while there is evidence for the presence of water molecules between heme *a* and the BNC as well as along the proton channels. Accordingly, we used variable dielectric constants by setting $D = 4$ for ε_{23} and $D = 20$ for the other couplings. With these geometric constraints (see Fig. 3A) and dielectric constants, one obtains $\varepsilon_{12} \leq 2.2$ kcal/mol, $\varepsilon_{13} \geq -1.1$ kcal/mol, and $\varepsilon_{23} \geq -18.5$ kcal/mol.

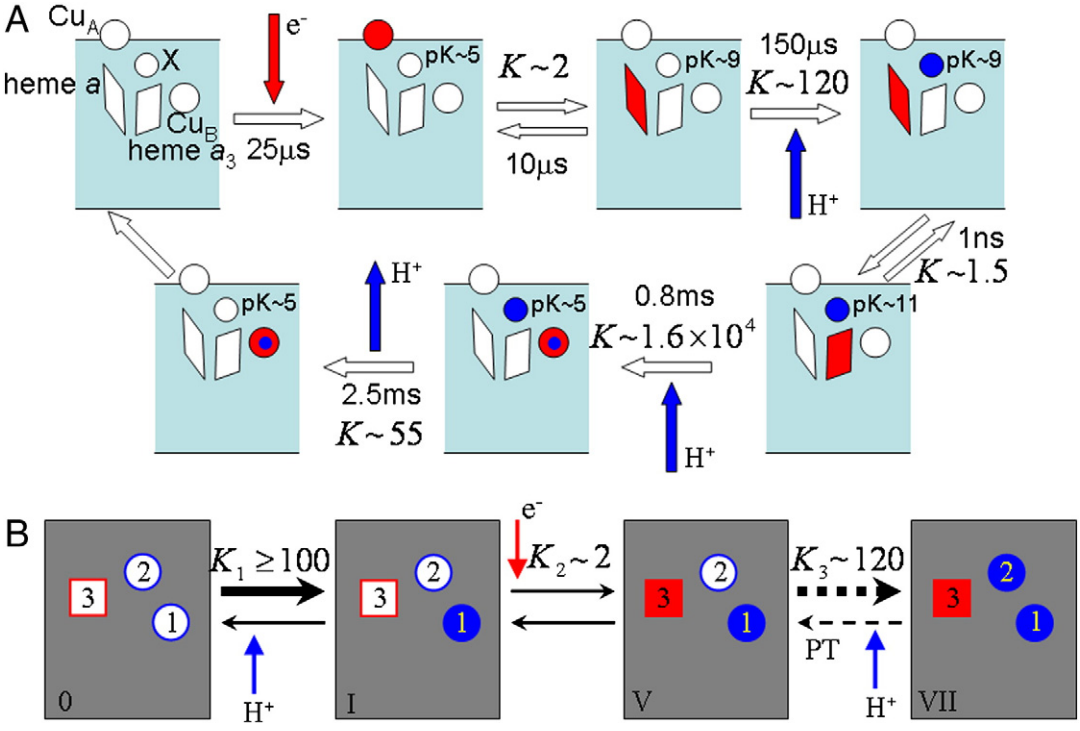

Fig. 4. CcO reaction cycle. (A) Measured equilibrium constants and rates along a proposed reaction sequence in the absence of membrane potential [25]. Electron and proton sites are represented as red squares and blue circles, respectively. (B) Corresponding reaction steps of the three-site model with experimental equilibrium constants. The dashed arrows in the last reaction indicate that the reaction is a two-step process consisting of the internal pT followed by the uptake of a proton from the N side.
Adapted from Fig. 2 of Ref. [42].

Equilibrium constants of key reaction steps have been measured as shown in Fig. 4A [25]. We identified corresponding reaction steps in our three-site kinetic model as presented in Fig. 4B, and imposed the equilibrium constants in optimizing the pumping efficiency in the model parameter space. As more experimental values become available and complex kinetic models, such as a five-state model, can reasonably be adopted, constraining some of the parameter values remains a straightforward procedure.

6.3. Proton pumping solutions and pump cycles

We found that even in the presence of experimental thermodynamic constraints on the parameter values it was relatively easy to find pumping solutions with high efficiency [42]. Fig. 5 shows the pumping efficiency as a function of the opposing membrane potential for a set of randomly picked solutions found by MC optimization in the parameter space. All thermodynamic constraints imposed above are satisfied by these solutions. The physical characteristics of the pumping solutions are diverse, in which some of them lose the pumping ability at membrane voltages of 100 mV, while others can pump protons at voltages as high as 200 mV, close to the mitochondrial membrane potential. It is remarkable that, in contrast to the original restricted three-site model [41], three-site models with kinetic gating are able to maintain a pumping efficiency of nearly 100% at voltages of >100 mV for a broad range of parameter values.

Fig. 5B presents the thermodynamic efficiency γ as a function of the membrane potential from the same solutions as in Fig. 5A. The thermodynamic efficiency lies between 20% and 60% in the range of membrane voltages from 100 mV to 200 mV, with peak efficiencies of ~60% at ~200 mV. The thermodynamic efficiency becomes negative at higher voltages, indicating that proton leakage from the P side to the N side overpowers the pumping flux as well as the product flux (i.e., $\eta<-1$; see below). Interestingly, a couple of models yield almost constant thermodynamic efficiency at $V_m>200$ mV.

The pumping solutions can be further characterized by identifying dominant reaction cycles. Only some of the cycles are coupled to pumping, with a majority of futile cycles resulting in product formation without proton pumping. For efficient pumping, the flux through these futile cycles must be suppressed. Within the three-site model, one can draw seven possible pump cycles that contain pumping steps. Fluxes are calculated for each pump cycle, and the cycle that yields the maximum flux is designated as dominant for a particular model [40]. Among the seven pump cycles, we observed that only five pump cycles are dominant in at least one model [42]. After comparing the electron up-take rates among the five cycles with experimental observations [25,63,64], we concluded that the two cycles shown in Fig. 6 are consistent with what is observed experimentally in CcO [42]. The major difference in the two cycles is the mechanism of the pumping step from site 2 to the P side. In cycle 5, a proton taken up from the N side to site 1 repels the proton in the site 2 to the P side; in contrast, there is no such repulsion that drives the proton in site 2 to the P side in cycle 4.

6.4. Kinetic gating for efficient proton pumping

What makes such simple models efficient proton pumps? A careful examination of the two dominant cycles presented in Fig. 6 shows that they compete with possible "slip" cycles in which product is formed without pumping. For example, in cycle 4 product formation at microstate V (i.e., the step V→0; dashed arrow) can lead to a slip cycle (0→I→V→0) in which product is formed before a proton is transferred to the pump site. Similarly, in cycle 5 the step II→I (proton back-flow from site 2 to site 1; dashed arrow) leads to a slip cycle (I→V→VI→VII→II→I) without pumping. The same slip cycle can be observed in cycle 4. Efficiency of pumping thus requires that such slip cycles are suppressed.

One of the key contributors to the improved pumping efficiency compared to the earlier models [41] is the ratio of intrinsic rates of the internal pT between sites 1 and 2 in the reduced state, κ^{r}_{pT}, (site 3 occupied) and oxidized state, κ^{o}_{pT}, (site 3 empty). Specifically, models with cycles 4 and 5 as dominant pump cycles were found to have κ^{r}_{pT} 10^6 times larger than κ^{o}_{pT} [42], as schematically illustrated in Fig. 7. Note that the dependence of the intrinsic pT rates on the microstates does not violate the detailed balance condition. In the earlier study the intrinsic rates were constrained, resulting in low efficiency [41]. The control of the intrinsic pT rates by an electron thus emerged as one of the contributors to the higher pumping efficiency [42]. The enhancement of the intrinsic pT rate in the reduced state accelerates the internal pT from site 1 to site 2 (step V→VI), but in comparison reduces the proton back-flow from site 2 to site 1 in the oxidized state (step II→I) to prevent proton leakage. Similarly, intrinsic product formation rates were shown to depend strongly on the protonation state of the pump site [42]. The intrinsic product formation rate in the presence of a proton in the pump site, κ^{+}_{PR}, was found to be much faster (~10^4 times) than that in the absence of a proton, κ^{0}_{PR}, as illustrated in Fig. 7 (bottom panel). Such "kinetic gating" is crucial to prevent any slip cycles or proton leakage from dominating in the models.

A combination of kinetic gating and a strong energetic bias (through pK_a's and mid-point potentials) ensure that a proton in site 1 is transferred to the pump site upon reduction of the electron site before forming a product. A fast proton up-take from the N side, combined with the strong electrostatic coupling between an electron and a proton in the pump site, blocks the pump proton from being

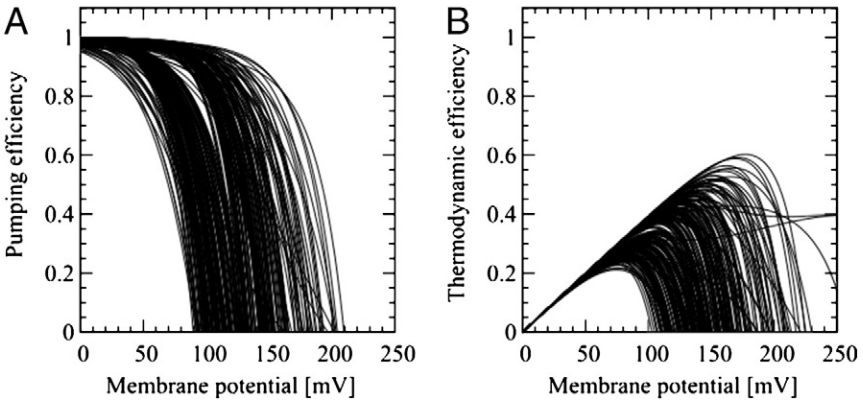

Fig. 5. (A) Pumping efficiency η and (B) thermodynamic efficiency γ as a function of the opposing membrane potential for proton-pumping solutions of the three-site model obtained via MC optimization. These solutions satisfy the thermodynamic equilibrium constants shown in Fig. 4 at zero membrane potential.

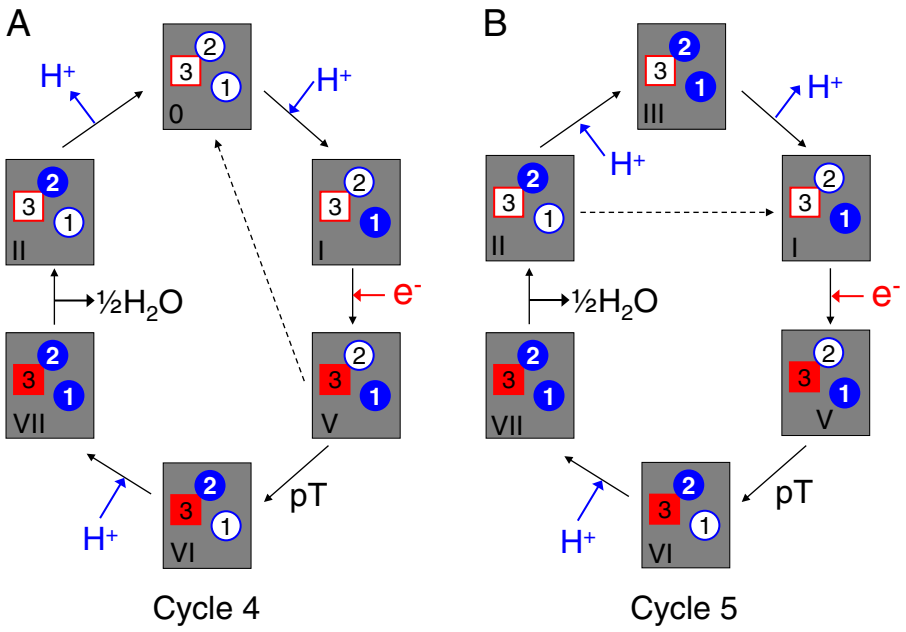

Fig. 6. Two dominant pump cycles. The dashed arrows indicate the formation of possible "slip" cycles in which a product is formed without proton pumping.

transferred back to site 1. Upon product formation, the absence of an electron in the electron site then reduces the intrinsic pT rate so that the pump proton can be transferred to the P side without (cycle 4) or with (cycle 5) the repulsive interaction from a proton at site 1.

Does CcO employ such kinetic gating to boost the pumping efficiency? And if so, what is the molecular origin of such gating? One should note that the analysis of master-equation models does not address the underlying microscopic mechanism. But the observed gating mechanism matches the predictions of the water-gated model of proton pumping by CcO [21] and more recent analyses of the pump mechanism [9,65,66]. In the water-gated model, a branched chain of water molecules inside a hydrophobic cavity next to the BNC [19,67,68] is thought to serve as an efficient proton conducting wire [69]. With heme *a* reduced, in molecular dynamics (MD) simulations the water-chain was found to be oriented from Glu 242 to the pump site [21], so that a proton from Glu 242 is easily transferred to the pump site. In contrast, reduction of the BNC orientated the water hydrogen bonds from Glu 242 to the BNC, thus facilitating pT to the active site for product formation. Moreover, the magnitude of the gating effect observed in the models, with a rate enhancement by a factor of ~10^6, corresponds to a drop in the barrier for pT by ~8.3 kcal/mol, a value close to the 7.1 kcal/mol predicted by Siegbahn and Blomberg [65]. The kinetic gating predicted by the master-equation models thus appears to be realizable microscopically.

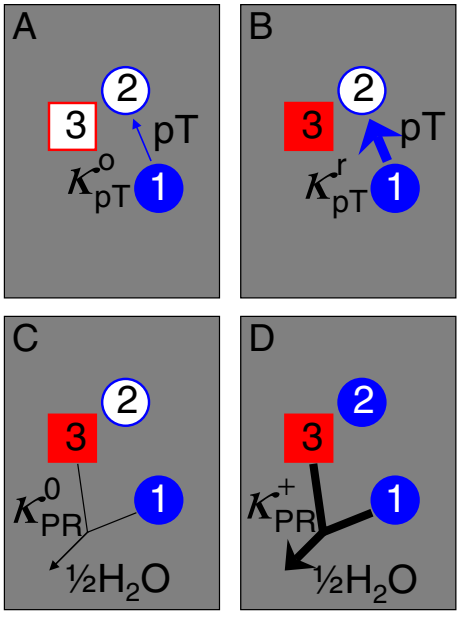

Fig. 7. Schematic drawing of kinetic gating. (A) and (B) illustrate the rate enhancement of the internal pT by the electron in site 3, while (C) and (D) depict the enhancement in the product formation rate by the proton in the pump site.

6.5. Mechanism of Glu valve

On the basis of the structure [12], modeling [67,68], and MD simulations [26], it has been suggested that the sidechain of Glu 242 shuttles between a state protonically connected to the D channel, and a state connected to the BNC and the pump site. Recent MD simulations [44] showed that this Glu motion depends on the protonation state, suggesting a possible functional role as a proton valve. The unprotonated Glu 242 remains predominantly in a "down" conformation in which its side chain points toward the N side, facilitating the uptake of a proton. Upon protonation, the "up" conformation, in which the side chain of Glu 242 is swung toward the P side by approximately 4 Å, is populated. This enables the internal pT to the pump site. Such a protonation-dependent conformational change helps block proton leakage from the pump site to Glu 242, where the unprotonated Glu 242 remains in the "safe" down conformation, ready for reprotonation.

To see if the Glu valve mechanism is thermodynamically allowed, and if it indeed improves the efficiency, we introduce a protonation-dependent conformation at the proton site 1 of our three-site model. The resulting additional kinetic reactions are presented in Fig. 8A, in which site 1 has two conformational states, down (1^d) and up (1^u). Proton uptake from the N side is possible only to the down conformation, whereas the internal pT can occur only between the up conformation of site 1 and site 2. Product can be formed only when the up conformation of site 1 and electron site 3 are simultaneously occupied.

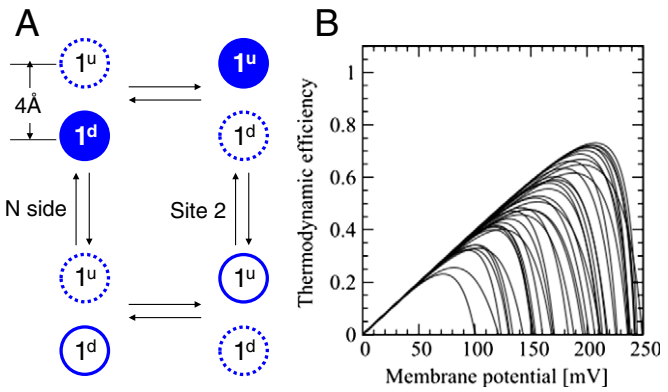

Fig. 8. Glu valve model. (A) Kinetic diagram of the Glu valve model. Glu has $2\times2=4$ states: two conformational states, up and down, as indicated by the two stacked circles, with the solid border indicating an occupied state; and two proton occupancy states, protonated (filled circle) and unprotonated (empty circle). The up (down) arrows represent the proton uptake (release). The left (right) arrows indicate transitions to the down (up) state. Only in the occupied up state can the proton be transferred internally to site 2, or used for product formation (when the electron site is occupied as well). (B) Thermodynamic efficiency γ of the kinetic Glu valve model as a function of membrane potential.

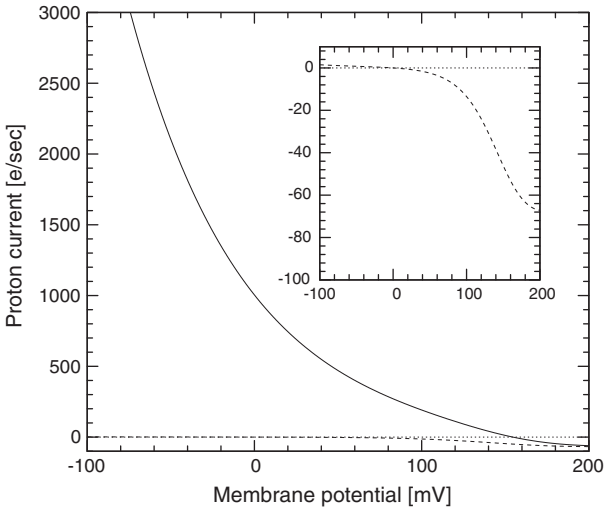

Fig. 9. Proton leakage in an optimized three-site model. The main panel shows proton currents as a function of assisting (negative) and opposing (positive) membrane potential under turnover conditions (solid line) and in the absence of product formation (dashed line). The inset shows a zoom-in of the proton leak current without turnover.

Geometrically, the up conformation lies above the down conformation by 4 Å in accordance with the MD data, making their equilibrium sensitive to membrane potentials. Note that the Glu valve model differs from a four-site model with an extra proton site, since in the latter the down and up sites could be occupied simultaneously by protons.

As above, the thermodynamic constraints are applied to the model during the MC optimization for finding pumping solutions. We observe that the Glu valve improves the pumping efficiency from the original three-site model. In particular, as shown in Fig. 8B, the thermodynamic efficiency approaches 80% even at membrane voltages >200 mV. In models that show pumping, the down conformation has a 1–6 kcal/mol lower intrinsic free energy than the up conformation, preferring the down conformation when site 1 is unprotonated. The range of free energy differences between up and down conformers is also consistent with the MD results [44,70]. The Glu valve improves the pumping efficiency by further blocking the proton-leak current through the pump site and site 1, with site 1 preferentially in a down conformation that is protonically disconnected from site 2.

6.6. Leak currents

The prevention of leak currents is indeed essential for the efficiency of a proton pump. So far, we have only considered the case of steady turnover, with an unlimited supply of electrons, protons, and oxygen as reactants. However, the pump should also prevent leak currents in the absence of turnover, where the pump function is completely lost. In Fig. 9, we compare the pump and leak currents with and without product formation. Results are shown for an optimized 3-site model that pumps up to a voltage of ~155 mV. We find that under conditions of normal load of membrane potentials between 0 and 200 mV, the leak currents remain small even in the absence of turnover compared to pump currents at ~100 mV. Interestingly, the particular model is also well sealed against leakage at negative membrane potentials in the absence of turnover.

6.7. Effects of D-channel mutations

Kinetic models can provide insight into the effects of mutations on the pumping efficiency. Experimentally, the N98D mutation introducing an aspartic acid into the D-channel between Glu 242 and the N side of the membrane resulted in an interesting phenotype in which the enzymatic activity of the WT is retained but the proton-pumping ability is lost [71,72]. This D-channel mutation can be easily incorporated into the optimized three-site models by introducing an additional proton site between the N side and proton site 1. By changing the intrinsic free energy of this extra site, but leaving the parameters associated with all other sites unchanged, one can qualitatively mimic the introduction of the ionizable residue N98D into the D channel [42]. We found that the majority of the models dominated by cycle 4 pump protons nearly as efficiently as the original three-site models, but those dominated by cycle 5 lose their pumping ability, while retaining about half the enzymatic activity of the original model. This behavior of models dominated by cycle 5 is qualitatively consistent with the experimental observations. The main cause for the lack of pumping in the N98D mutants seems to be an effective shutdown of the internal pT from site 1 to site 2 [42].

7. Concluding remarks

The kinetic master-equation approach provides a powerful tool to study molecular machines operating far from equilibrium. By carefully designing models and assigning appropriate rates, one can gain relevant insight into the molecular mechanisms underlying their function. In particular, we developed kinetic models to elucidate the mechanism of proton pumping by CcO driven by redox chemistry. Experimental thermodynamic and kinetic data as well as mutagenesis results can easily be incorporated into the models. Similarly, results of electrostatics and quantum-chemical calculations, and of MD simulations can be used in the design and parameterization of the model [18,19,26,27,29,44,65–70,73–78]. Studies of the simplest three-site models revealed basic principles of the redox-coupled proton pump [41–43]. These master-equation models showed in particular that kinetic gating is critical to achieving high pumping efficiency. The required rate enhancement of the internal pT from Glu 242 to the pump site, mediated by the electron in heme *a*, is consistent with the concept of the water-gate model [21].

The thermodynamic efficiency of most three-site models lies between 20% and 60%, well below the efficiency of CcO operating at physiological condition. As seen in the analysis of a four-site model with an additional electron site [41], increasing the complexity of the kinetic models improved the efficiency. This result suggests that the complexity of the electron and proton pathways in CcO is crucial

in its operation at such a high efficiency. We showed here that the inclusion of a Glu-valve, in which Glu 242 switches between a high-population down conformer and a low-population up conformer, indeed resulted in an increased thermodynamic efficiency of almost 80%. Thus the analysis of kinetic models with greater complexity by including additional redox centers as well as proton sites may well be justified. Although the development of such complex kinetic models requires additional efforts, not least on the experimental side, they should prove useful in identifying the general principles of CcO function and in creating blueprints for artificial redox-driven molecular machines.

Our study addresses a question central to proton pumping: how can gating of the proton flow be achieved when all microscopic processes are fully reversible. The modulation of the barriers governing the rates of microscopic transitions is often presumed to be essential for gating [78,79]. However, in ref. [41] we used a simple 3-site model to show that proton pumping is possible even without any barrier modulation, as long as reactant and product concentrations are out of equilibrium. We could show that already a modest-sized network model with two proton sites and one electron site, resulting in eight microscopic states, provides sufficient complexity that an exergonic reaction (the reduction of oxygen to water) can be coupled to an endergonic reaction (the pumping of protons against an electrochemical potential). In this simplest 3-site model, gating was achieved entirely by modulating the proton and electron affinities of the microscopic states, and without state-dependent modulation of the kinetic prefactors. The analysis of kinetic master-equation models thus shows that barrier modulation is not essential for gating, as long as the microscopic system has sufficient chemical complexity.

Nevertheless, the kinetic gating associated with barrier modulation can greatly increase the efficiency of pumping [41,42]. Ref. [41] showed that the pumping efficiency of a master-equation model can be improved either by increasing the number of electron and proton sites, and thus its chemical complexity, or by modulating the kinetic prefactors κ_{ij} of key microscopic transitions. Ref. [42] subsequently showed that kinetic gating of the proton transfers from Glu 242 to the pump site and into the BNC for chemistry is key to the high pumping efficiency of CcO, consistent with the water-gated mechanism of pumping [21]. Here we showed that the Glu valve of ref. [44] further improves the efficiency by preventing proton leakage. In our model of the Glu valve, detailed balance is satisfied, i.e., the up-down shuttling and the pT reactions are microscopically reversible and satisfy Eq. (2). This analysis thus addresses a concern raised in Ref. [79] that "an isomerization of a side chain by itself cannot establish a gate (because of microscopic reversibility)." In an open system of sufficient complexity (of the underlying network of chemical reaction steps), a device such as the Glu valve can serve effectively as a gate that increases the overall efficiency. So, while proton pumping can be achieved even in a simple model without barrier modulation [41], increased complexity, kinetic gating, and the Glu valve all help improve the efficiency of the pump.

Nevertheless, one must keep in mind that the master equation approach employed here does, by itself, not address the question how a particular element is realized atomistically. Based on their recent MD simulations of CcO [80], Yang and Cui questioned both the water-gate and Glu valve mechanisms as gating elements. They argue that with their refined dielectric model the orientational preferences of both the active site water and of the conserved glutamic acid are substantially altered. Clearly, this is a serious concern that deserves further investigation by simulation and, ultimately, by experiment. Interestingly, though, their finding that the Glu-242 side chain (bovine numbering) is strongly biased to pointing up into the BNC (counter to what is seen in the crystal structures) could also result in a gate functioning similar to the one studied in Fig. 8, by breaking the connectivity between the active site region and the D channel in a way that depends on the charge state of the active site region.

So while the barrier modulation involved in kinetic gating improves the pumping efficiency dramatically within our simplified kinetic models, uncovering the underlying molecular mechanisms requires further experimental investigations. Furthermore, it is still an open question whether such barrier-modulating mechanisms are necessary to achieve the high pumping efficiency of actual oxidase. Earlier studies using a more complex four-site model showed substantially improved pumping efficiency [41]. Preliminary studies using a five-site model that includes a more detailed rendering of the BNC (Fig. 3B) indicate that even higher efficiencies are possible in principle. Overall, by expanding the number of states in more complex kinetic networks, "gates" become regular parts of the system without the need of explicit barrier modulation.

The kinetic master-equation approach employed here can readily be applied also to other molecular machines, e.g., motor proteins. Similar approaches were already taken in studying the motion of motor proteins [59], but our approach differs from these with respect to the explicit inclusion of the chemical reaction step that effectively breaks detailed balance in an open system with given reactant concentrations. Following a similar route, models designed to couple ATP hydrolysis and the unidirectional motion of motor proteins may reveal important substeps as well as the mechanisms of motor-protein motion.

Acknowledgements

We thank Prof. Mårten Wikström and Dr. Ville Kaila for many insightful and stimulating discussions. G.H. is supported by the Intramural Research Program of the National Institute of Diabetes and Digestive and Kidney Diseases, National Institutes of Health.

References

[1] M.K.F. Wikström, Proton pump coupled to cytochrome-c oxidase in mitochondria, Nature 266 (1977) 271–273.
[2] G.T. Babcock, M. Wikström, Oxygen activation and the conservation of energy in cell respiration, Nature 356 (1992) 301–309.
[3] S. Ferguson-Miller, G.T. Babcock, Heme/copper terminal oxidases, Chem. Rev. 96 (1996) 2889–2907.
[4] D. Zaslavsky, R.B. Gennis, Proton pumping by cytochrome oxidase: progress, problems and postulates, Biochim. Biophys. Acta, Bioenerg. 1458 (2000) 164–179.
[5] P. Brzezinski, G. Larsson, Redox-driven proton pumping by heme–copper oxidases, Biochim. Biophys. Acta, Bioenerg. 1605 (2003) 1–13.
[6] M. Wikström, Cytochrome *c* oxidase: 25 years of the elusive proton pump, Biochim. Biophys. Acta, Bioenerg. 1655 (2004) 241–247.
[7] E. Khalimonchuk, G. Rödel, Biogenesis of cytochrome *c* oxidase, Mitochondrion 5 (2005) 363–388.
[8] G. Brändén, R.B. Gennis, P. Brzezinski, Transmembrane proton translocation by cytochrome *c* oxidase, Biochim. Biophys. Acta, Bioenerg. 1757 (2006) 1052–1063.
[9] M. Wikström, M.I. Verkhovsky, Mechanism and energetics of proton translocation by the respiratory heme–copper oxidases, Biochim. Biophys. Acta, Bioenerg. 1767 (2007) 1200–1214.
[10] P. Brzezinski, R.B. Gennis, Cytochrome *c* oxidase: exciting progress and remaining mysteries, J. Bioenerg. Biomembr. 40 (2008) 521–531.
[11] T. Tsukihara, K. Shimokata, Y. Katayama, H. Shimada, K. Muramoto, H. Aoyoma, M. Mochizuki, K. Shinzawa-Itoh, E. Yamashita, M. Yao, Y. Ishimura, S. Yoshikawa, The low-spin heme of cytochrome *c* oxidase as the driving element of the proton-pumping process, Proc. Natl. Acad. Sci. U. S. A. 100 (2003) 15304–15309.
[12] S. Iwata, C. Ostermeier, B. Ludwig, H. Michel, Structure at 2.8-Angstrom resolution of cytochrome-c-oxidase from *Paracoccus denitrificans*, Nature 376 (1995) 660–669.
[13] T. Tsukihara, H. Aoyama, E. Yamashita, T. Tomizaki, H. Yamaguchi, K. Shinzawa-Itoh, R. Nakashima, R. Yaono, S. Yoshikawa, Structures of metal sites of oxidized bovine heart cytochrome-c-oxidase at 2.8 Angstrom, Science 269 (1995) 1069–1074.
[14] R.B. Gennis, How does cytochrome oxidase pump protons? Proc. Natl. Acad. Sci. U. S. A. 95 (1998) 12747–12749.
[15] V.Y. Artzatbanov, A.A. Konstantinov, V.P. Skulachev, Involvement of intramitochondrial protons in redox reactions of cytochrome-a, FEBS Lett. 87 (1978) 180–185.
[16] S. Papa, N. Capitanio, G. Villani, A cooperative model for protonmotive heme–copper oxidases. The role of heme a in the proton pump of cytochrome *c* oxidase, FEBS Lett. 439 (1998) 1–8.
[17] H. Michel, Cytochrome *c* oxidase: catalytic cycle and mechanisms of proton pumping—a discussion, Biochemistry 38 (1999) 15129–15140.
[18] P.E.M. Siegbahn, M.R.A. Blomberg, M.L. Blomberg, Theoretical study of the energetics of proton pumping and oxygen reduction in cytochrome oxidase, J. Phys. Chem. B 107 (2003) 10946–10955.

[19] A.A. Stuchebrukhov, Electron transfer reactions coupled to proton translocation. Cytochrome oxidase, proton pumps, and biological energy transduction, J. Theory Comput. Chem. 2 (2003) 91–118.
[20] L. Qin, C. Hiser, A. Mulichak, R.M. Garavito, S. Ferguson-Miller, Identification of conserved lipid/detergent-binding sites in a high-resolution structure of the membrane protein cytochrome *c* oxidase, Proc. Natl. Acad. Sci. U. S. A. 103 (2006) 16117–16122.
[21] M. Wikström, M.I. Verkhovsky, G. Hummer, Water-gated mechanism of proton translocation by cytochrome *c* oxidase, Biochim. Biophys. Acta, Bioenerg. 1604 (2003) 61–65.
[22] K. Faxén, G. Gilderson, P. Ädelroth, P. Brzezinski, A mechanistic principle for proton pumping by cytochrome *c* oxidase, Nature 437 (2005) 286–289.
[23] I. Belevich, M.I. Verkhovsky, M. Wikström, Proton-coupled electron transfer drives the proton pump of cytochrome *c* oxidase, Nature 440 (2006) 829–832.
[24] M.H.M. Olsson, A. Warshel, Monte Carlo simulations of proton pumps: on the working principles of the biological valve that controls proton pumping in cytochrome *c* oxidase, Proc. Natl. Acad. Sci. U. S. A. 103 (2006) 6500–6505.
[25] I. Belevich, D.A. Bloch, N. Belevich, M. Wikström, M.I. Verkhovsky, Exploring the proton pump mechanism of cytochrome *c* oxidase in real time, Proc. Natl. Acad. Sci. U. S. A. 104 (2007) 2685–2690.
[26] R. Pomès, G. Hummer, M. Wikström, Structure and dynamics of a proton shuttle in cytochrome *c* oxidase, Biochim. Biophys. Acta 1365 (1998) 255–260.
[27] R.M. Henry, C.-H. Yu, T. Rodinger, R. Pomès, Functional hydration and conformational gating of proton uptake in cytochrome *c* oxidase, J. Mol. Biol. 387 (2009) 1165–1185.
[28] P. Mitchell, Coupling of phosphorylation to electron and hydrogen transfer by a chemi-osmotic type of mechanism, Nature 191 (1961) 144–148.
[29] D.M. Popović, A.A. Stuchebrukhov, Proton pumping mechanism and catalytic cycle of cytochrome *c* oxidase: Coulomb pump model with kinetic gating, FEBS Lett. 566 (2004) 126–130.
[30] R. Ballardini, V. Balzani, A. Credi, M.T. Gandolfi, M. Venturi, Artificial molecular-level machines: which energy to make them work? Acc. Chem. Res. 34 (2001) 445–455.
[31] M.G.L. van den Heuvel, C. Dekker, Motor proteins at work for nanotechnology, Science 317 (2007) 333–336.
[32] W.R. Browne, B.L. Feringa, Making molecular machines work, Nat. Nanotechnol. 1 (2006) 25–35.
[33] R. Eelkema, M.M. Pollard, J. Vicario, N. Katsonis, B.S. Ramon, C.W.M. Bastiaansen, D.J. Broer, B.L. Feringa, Nanomotor rotates microscale objects, Nature 440 (2006) 163-163.
[34] G. Oster, A. Perelson, A. Katchalsky, Network thermodynamics, Nature 234 (1971) 393–399.
[35] J. Schnakenberg, Network theory of microscopic and macroscopic behavior of master equation systems, Rev. Mod. Phys. 48 (1976) 571–585.
[36] H. Qian, Equations for stochastic macromolecular mechanics of single proteins: equilibrium fluctuations, transient kinetics, and nonequilibrium steady-state, J. Phys. Chem. B 106 (2002) 2065–2073.
[37] H. Qian, Open-system nonequilibrium steady state: statistical thermodynamics, fluctuations, and chemical oscillations, J. Phys. Chem. B 110 (2006) 15063–15074.
[38] R.D. Astumian, M. Bier, Fluctuation driven ratchets — molecular motors, Phys. Rev. Lett. 72 (1994) 1766–1769.
[39] R.D. Astumian, Thermodynamics and kinetics of a Brownian motor, Science 276 (1997) 917–922.
[40] T.L. Hill, Free Energy Transduction in Biology, Academic, New York, 1977.
[41] Y.C. Kim, M. Wikström, G. Hummer, Kinetic models of redox-coupled proton pumping, Proc. Natl. Acad. Sci. U. S. A. 104 (2007) 2169–2174.
[42] Y.C. Kim, M. Wikström, G. Hummer, Kinetic gating of the proton pump in cytochrome *c* oxidase, Proc. Natl. Acad. Sci. U. S. A. 106 (2009) 13707–13712.
[43] Y.C. Kim, L.A. Furchtgott, G. Hummer, Biological proton pumping in an oscillating electric field, Phys. Rev. Lett. 103 (2009) 4.
[44] V.R.I. Kaila, M.I. Verkhovsky, G. Hummer, M. Wikström, Glutamic acid 242 is a valve in the proton pump of cytochrome *c* oxidase, Proc. Natl. Acad. Sci. U. S. A. 105 (2008) 6255–6259.
[45] A.P. Somlyo, A.V. Somlyo, Signal-transduction and regulation in smooth-muscle, Nature 372 (1994) 231–236.
[46] B. Alberts, The cell as a collection of protein machines: preparing the next generation of molecular biologists, Cell 92 (1998) 291–294.
[47] B. Alberts, R. Miakelye, Unscrambling the puzzle of biological machines — the importance of the details, Cell 68 (1992) 415–420.
[48] R.D. Vale, R.J. Fletterick, The design plan of kinesin motors, Annu. Rev. Cell Dev. Biol. 13 (1997) 745–777.
[49] J. Howard, Molecular motors: structural adaptations to cellular functions, Nature 389 (1997) 561–567.
[50] D.J. Sharp, G.C. Rogers, J.M. Scholey, Microtubule motors in mitosis, Nature 407 (2000) 41–47.
[51] G. Yellen, The voltage-gated potassium channels and their relatives, Nature 419 (2002) 35–42.
[52] E. Gouaux, R. MacKinnon, Principles of selective ion transport in channels and pumps, Science 310 (2005) 1461–1465.
[53] M. Yoshida, E. Muneyuki, T. Hisabori, ATP synthase — a marvellous rotary engine of the cell, Nat. Rev. Mol. Cell Biol. 2 (2001) 669–677.
[54] M.E. Fisher, A.B. Kolomeisky, Simple mechanochemistry describes the dynamics of kinesin molecules, Proc. Natl. Acad. Sci. U. S. A. 98 (2001) 7748–7753.
[55] M.E. Fisher, Y.C. Kim, Kinesin crouches to sprint but resists pushing, Proc. Natl. Acad. Sci. U. S. A. 102 (2005) 16209–16214.
[56] Y.C. Kim, M.E. Fisher, Vectorial loading of processive motor proteins: implementing a landscape picture, J. Phys. Condens. Matter 17 (2005) S3821–S3838.
[57] D.A. Proshlyakov, M.A. Pressler, C. DeMaso, J.F. Leykam, D.L. DeWitt, G.T. Babcock, Oxygen activation and reduction in respiration: involvement of redox-active tyrosine 244, Science 290 (2000) 1588–1591.
[58] E.A. Gorbikova, M. Wikström, M.I. Verkhovsky, The protonation state of the cross-linked tyrosine during the catalytic cycle of cytochrome *c* oxidase, J. Biol. Chem. 283 (2008) 34907–34912.
[59] A.B. Kolomeisky, M.E. Fisher, Molecular motors: a theorist's perspective, Annu. Rev. Phys. Chem. 58 (2007) 675–695.
[60] E. von Kitzing, D.M. Soumpasis, Electrostatics of a simple membrane model using green's functions formalism, Biophys. J. 71 (1996) 795–810.
[61] S. Szaraz, D. Oesterhelt, P. Ormos, pH-induced structural-changes in bacteriorhodopsin studied by Fourier-transform infrared-spectroscopy, Biophys. J. 67 (1994) 1706–1712.
[62] A. Namslauer, A. Aagaard, A. Katsonouri, P. Brzezinski, Intramolecular proton-transfer reactions in a membrane-bound proton pump: the effect of pH on the peroxy to ferryl transition in cytochrome *c* oxidase, Biochemistry 42 (2003) 1488–1498.
[63] L.P. Pan, S. Hibdon, R.Q. Liu, B. Durham, F. Millett, Intracomplex electron-transfer between ruthenium-cytochrome-c derivatives and cytochrome-c-oxidase, Biochemistry 32 (1993) 8492–8498.
[64] L.M. Geren, J.R. Beasley, B.R. Fine, A.J. Saunders, S. Hibdon, G.J. Pielak, B. Durham, F. Millett, Design of a ruthenium cytochrome-c derivative to measure electron-transfer to the initial acceptor in cytochrome-c-oxidase, J. Biol. Chem. 270 (1995) 2466–2472.
[65] P.E.M. Siegbahn, M.R.A. Blomberg, Energy diagrams and mechanism for proton pumping in cytochrome *c* oxidase, Biochim. Biophys. Acta, Bioenerg. 1767 (2007) 1143–1156.
[66] P.E.M. Siegbahn, M.R.A. Blomberg, Proton pumping mechanism in cytochrome *c* oxidase, J. Phys. Chem. A 112 (2008) 12772–12780.
[67] S. Riistama, G. Hummer, A. Puustinen, R.B. Dyer, W.H. Woodruff, M. Wikström, Bound water in the proton translocation mechanism of the haem–copper oxidases, FEBS Lett. 414 (1997) 275–280.
[68] I. Hofacker, K. Schulten, Oxygen and proton pathways in cytochrome *c* oxidase, Proteins 30 (1998) 100–107.
[69] C. Dellago, M.M. Naor, G. Hummer, Proton transport through water-filled carbon nanotubes, Phys. Rev. Lett. 90 (2003) 4.
[70] V.R.I. Kaila, M. Verkhovsky, G. Hummer, M. Wikström, Prevention of leak in the proton pump of cytochrome *c* oxidase, Biochim. Biophys. Acta, Bioenerg. 1777 (2008) 890–892.
[71] U. Pfitzner, K. Hoffmeier, A. Harrenga, A. Kannt, H. Michel, E. Bamberg, O.M.H. Richter, B. Ludwig, Tracing the D-pathway in reconstituted site-directed mutants of cytochrome *c* oxidase from *Paracoccus denitrificans*, Biochemistry 39 (2000) 6756–6762.
[72] A. Namslauer, A.S. Pawatet, R. Gennis, P. Brzezinski, Redox-coupled proton translocation in biological systems: proton shuttling in cytochrome *c* oxidase, Proc. Natl. Acad. Sci. U. S. A. 100 (2003) 15543–15547.
[73] A. Kannt, C.R.D. Lancaster, H. Michel, The coupling of electron transfer and proton translocation: electrostatic calculations on *Paracoccus denitrificans* cytochrome *c* oxidase, Biophys. J. 74 (1998) 708–721.
[74] E. Olkhova, M.C. Hutter, M.A. Lill, V. Helms, H. Michel, Dynamic water networks in cytochrome *c* oxidase from *Paracoccus denitrificans* investigated by molecular dynamics simulations, Biophys. J. 86 (2004) 1873–1889.
[75] S.A. Seibold, D.A. Mills, S. Ferguson-Miller, R.I. Cukier, Water chain formation and possible proton pumping routes in *Rhodobacter sphaeroides* cytochrome *c* oxidase: a molecular dynamics comparison of the wild type and R481K mutant, Biochemistry 44 (2005) 10475–10485.
[76] J.C. Xu, G.A. Voth, Redox-coupled proton pumping in cytochrome *c* oxidase: further insights from computer simulation, Biochim. Biophys. Acta, Bioenerg. 1777 (2008) 196–201.
[77] N. Ghosh, X. Prat-Resina, M.R. Gunner, Q. Cui, Microscopic pK_a analysis of Glu286 in cytochrome *c* oxidase: toward a calibrated molecular model, Biochemistry 48 (2009) 2468–2485.
[78] A.V. Pisliakov, P.K. Sharma, Z.T. Chu, M. Haranczyk, A. Warshel, Electrostatic basis for the unidirectionality of the primary proton transfer in cytochrome *c* oxidase, Proc. Natl. Acad. Sci. U. S. A. 105 (2008) 7726–7731.
[79] P. Brzezinski, A.-L. Johansson, Variable proton-pumping stoichiometry in structural variants of cytochrome *c* oxidase, Biochim. Biophys. Acta, Bioenerg. 1797 (2010) 710–723.
[80] S. Yang, Q. Cui, Glu-286 rotation and water wire reorientation are unlikely the gating elements for proton pumping in cytochrome *c* oxidase, Biophys. J. 101 (2011) 61–69.